IOP PUBLISHING PHYSICS IN MEDICINE AND BIOLOGY

Phys. Med. Biol. **53** (2008) 6377–6394 doi:10.1088/0031-9155/53/22/008

Preliminary *in vivo* atherosclerotic carotid plaque characterization using the accumulated axial strain and relative lateral shift strain indices

Hairong Shi[1], **Carol C Mitchell**[2], **Matthew McCormick**[1,3], **Mark A Kliewer**[4], **Robert J Dempsey**[5] **and Tomy Varghese**[1,3,6]

[1] Department of Medical Physics, The University of Wisconsin-Madison, Madison, WI-53706, USA
[2] Ultrasound Technology School, The University of Wisconsin-Madison, Madison, WI-53706, USA
[3] Department of Biomedical Engineering, The University of Wisconsin-Madison, Madison, WI-53706, USA
[4] Department of Radiology, The University of Wisconsin-Madison, Madison, WI-53706, USA
[5] Department of Neurological Surgery, The University of Wisconsin-Madison, Madison, WI-53706, USA

E-mail: tvarghese@wisc.edu

Received 3 January 2008, in final form 19 September 2008
Published 21 October 2008
Online at stacks.iop.org/PMB/53/6377

Abstract

In this paper, we explore two parameters or strain indices related to plaque deformation during the cardiac cycle, namely, the maximum accumulated axial strain in plaque and the relative lateral shifts between plaque and vessel wall under *in vivo* clinical ultrasound imaging conditions for possible identification of vulnerable plaque. These strain indices enable differentiation between calcified and lipidic plaque tissue utilizing a new perspective based on the stiffness and mobility of the plaque. In addition, they also provide the ability to distinguish between softer plaques that undergo large deformations during the cardiac cycle when compared to stiffer plaque tissue. Soft plaques that undergo large deformations over the cardiac cycle are more prone to rupture and to release micro-emboli into the cerebral bloodstream. The ability to identify vulnerable plaque, prone to rupture, would significantly enhance the clinical utility of this method for screening patients. We present preliminary *in vivo* results obtained from ultrasound radio frequency data collected over 16 atherosclerotic plaque patients before these patients undergo a carotid endarterectomy procedure. Our preliminary *in vivo* results indicate that the maximum accumulated axial strain over a cardiac cycle and the maximum relative lateral shift or displacement of the plaque are useful strain indices that provide differentiation between soft and calcified plaques.

[6] Author to whom any correspondence should be addressed.

Introduction

Carotid artery atherosclerosis and its relationship to embolic stroke has been an area of considerable research focus due to the devastating effects of emboli. A major endpoint of most carotid atherosclerosis studies has been measurable stroke manifested generally by motor, sensory, speech and vision deficits. Doppler studies, searching for carotid emboli distal to symptomatic carotid plaques, suggest that at the time of presentation with a motor transient ischemic attack, multiple other clinically unrecognized emboli are passing to the brain (Droste *et al* 1996). Studies of coronary and carotid surgery patients have also shown a significant number of cerebral emboli occurring and flowing up the carotids during these procedures (Siebler *et al* 1996). The need to look at the pathophysiology of atherosclerotic disease beyond simple parameters of degree of stenosis or irregularity of surface has led us to look at the structural stability of these plaques using the strain imaging parameters or indices derived from displacement and strain images, namely, the maximum accumulated axial strain and relative lateral shift, as potential markers for vulnerable plaque.

Plaque vulnerability is assumed to be determined primarily by the mechanical (elastic) properties of the vessel wall and the plaque composition (Richardson *et al* 1989, Fuster *et al* 1990, Gronholdt 1999). The structural stability of a carotid plaque is a result of its chemical composition, cellular material and new vessel formation. Various studies have indicated that the pulsatile pressure induced due to blood flow may rupture the thin cap overlying fatty tissue (or lipid-rich lesions) on the plaque, which may lead to subsequent thrombosis and plaque rupture (Richardson *et al* 1989, Richardson 2002). Techniques that are able to characterize the elastic properties of plaque may therefore provide clinical information that may have a significant impact on patient care. Characterization of the plaque composition in vascular tissue can also significantly help in the selection of appropriate interventional techniques to prevent plaque rupture.

Ultrasonic tissue characterization parameters such as the scatterer size and attenuation coefficient parameters have been explored previously by a large number of researchers for plaque characterization (Wilson *et al* 1994, Bridal *et al* 1997, Noritomi *et al* 1997, Nair *et al* 2002, Waters *et al* 2003, Shi *et al* 2008). Fewer researchers, thus far, have focused on evaluating the elastographic properties of atherosclerotic plaque (de Korte *et al* 2000, de Korte and van der Steen 2002, Baldewsing *et al* 2005, Maurice *et al* 2007, Ribbers *et al* 2007, Schmitt *et al* 2007). Imaging of tissue elastic parameters for diagnosis of pathological changes in biological tissue is rapidly gaining attention because of the ability to provide noninvasive and additional new information (Wilson and Robinson 1982, Krouskop *et al* 1987, Bertrand *et al* 1989, Parker *et al* 1990, 1996, Yamakoshi *et al* 1990, O'Donnell *et al* 1991, 1994, Ophir *et al* 1991, 2000, Cespedes 1993, Talhami *et al* 1994, Chen *et al* 1995, Gao *et al* 1996, Garra *et al* 1997, Konofagou and Ophir 1998, van der Steen *et al* 1998, de Korte *et al* 2000, Insana *et al* 2000, Walker *et al* 2000, Doyley *et al* 2001, Varghese *et al* 2001, Emelianov *et al* 2002, Nightingale *et al* 2002, Zhu and Hall 2002, Weitzel *et al* 2005, Rubin *et al* 2006). Reconstruction of the elastic moduli from the displacement or strain data has been reported as well (O'Donnell *et al* 1994, Sumi *et al* 1995, Kallel and Bertrand 1996).

However, most of the elastographic studies for plaque characterization were performed using intravascular ultrasound (IVUS) techniques on coronary arteries (de Korte *et al* 2000, de Korte and van der Steen 2002). de Korte *et al* (2000) performed detailed IVUS elastography studies for plaque characterization, along with *in vivo* evaluation on an Yucatan pig animal model (de Korte and van der Steen 2002). Leung *et al* (2006) performed *in vivo* IVUS elastography studies on human patients. Although IVUS provides higher spatial resolution, it also suffers from several problems associated with intravascular strain imaging in addition

to being an invasive procedure. For example, the angular dependence of insonification and reverberation artifacts makes IVUS images difficult to interpret, and the increased frequency-dependent attenuation slope (with higher center frequencies) reduces signal penetration in some cases. Moreover, catheter position artifacts also introduce strain estimation errors (Shi *et al* 2005). These problems affect the accuracy of the displacement and strain estimations performed.

Meanwhile, few *in vivo* elastographic studies have been performed on the carotid artery using clinical ultrasound systems equipped with linear array transducers (Maurice *et al* 2004, Shi *et al* 2006, Ribbers *et al* 2007, Schmitt *et al* 2007, Maurice *et al* 2008). Maurice *et al* (2004) utilized the Lagrangian strain estimator to estimate the partial Von Mises strain coefficient of vascular data acquired using a linear array transducer. Their simulation results indicate that the Von Mises coefficient can overcome mechanical artifacts and characterize the vessel wall. Ribbers *et al* (2007) utilized 2D displacement and strain to calculate radial and circumferential strain in the carotid artery for 12 subjects. They concluded that for cross-sectional strain imaging, both the radial and circumferential strains have to be estimated. In addition these radial and circumferential strains are not well aligned with the ultrasound beam for all regions leading to errors in strain interpretation. On the other hand, for longitudinal scans the radial strain and the ultrasound beam are aligned improving the ease of the strain interpretation. Golemati *et al* (2003) used 2D block matching to track carotid artery wall motion on B-mode images, where the expected cyclical motion of the artery wall along the radial direction was analyzed. Schmitt *et al* (2007) reported on the *in vivo* investigation of strain tensor components from both cross-sectional and longitudinal radio frequency data, from two healthy subjects and two patients with severe carotid stenoses using the Lagrangian method. While healthy subjects show similar modulus values, the strain and shear elastograms of heterogeneous plaques in patients reveal information about plaque size, composition and mechanical interactions such as the stress concentration between structures.

We have developed a novel 2D multi-level cross-correlation method to compute local displacement fields and strains in discontinuous media (Shi 2007, Shi and Varghese 2007). This algorithm is particularly suited for displacement and strain estimation for longitudinal scans of the carotid artery. Coarse displacement estimates are initially obtained using sub-sampled B-mode data using a multi-level pyramidal search algorithm. The coarse displacement estimates are then utilized to guide the high-resolution estimation on the lowest level of the pyramid containing the radio frequency (RF) echo signal data. This method combines advantages provided by the robustness of B-mode envelope tracking and the precision obtained using RF motion tracking to obtain high-resolution displacement and strain estimates.

In this paper, we evaluate the use of noninvasive carotid strain imaging for *in vivo* evaluation of plaque in the carotid artery of patients scheduled for a carotid endarterectomy procedure. We focus on two deformation parameters or indices, namely, the accumulated axial strain and the relative lateral shift between plaque and artery wall. We evaluate the variation in these two indices for calcified and non-calcified plaque identified from ultrasound B-mode images as hyperechoic regions with shadowing below and hypoechoic regions that occlude blood flow, respectively.

Materials and method

In vivo data acquisition

In vivo data acquisition on patients with carotid stenosis and plaque was performed at the University of Wisconsin-Madison Hospitals and Clinics, under a protocol approved by the

Table 1. B-mode and clinical features of the patients that were included in the *in vivo* strain imaging of the carotid artery.

No	Region of interest from B-mode image	Carotid (surgical) side	Symptomatic/ asymptomatic
1	Calcified	Right carotid	Asymptomatic
2	Calcified, hypoechoic	Right carotid	Asymptomatic
3	Calcified	Right carotid	Symptomatic
4	Hypoechoic	Right carotid	Asymptomatic
5	Calcified, hypoechoic	Right carotid	Asymptomatic
6	Hypoechoic	Left carotid	Symptomatic
7	Calcified, hypoechoic	Left carotid	Symptomatic
8	Hypoechoic	Left carotid	Symptomatic
9	Calcified, heterogeneous	Left carotid	Symptomatic
10	Hypoechoic	Left carotid	Questionable
11	Calcified	Right carotid	Asymptomatic
12	Calcified	Left carotid	Asymptomatic
13	Hypoechoic	Right carotid	Symptomatic
14	Calcified	Left carotid	Symptomatic
15	Hypoechoic	Left carotid	Symptomatic
16	Calcified	Right carotid	Symptomatic

UW-Madison Institutional Review Board (IRB) for data acquisition on human patients. Only patients who have already been scheduled for carotid endarterectomy for standard clinical indications were recruited to participate in this study. Ultrasound RF data were acquired on 16 patients who had consented to be part of this study. Patients were scanned using a Siemens Antares system (Siemens Ultrasound, Mountain View, CA, USA) equipped with the Axius direct ultrasound research interface (URI). In addition to the RF data acquisition, a complete carotid clinical ultrasound study was performed with color-flow Doppler imaging to determine regions and velocities of blood flow and to guide acquisition of ultrasound B-mode and RF data loops. Table 1 presents a database of the patients included in this study. The mean age of the patients was 69.2 ± 8.38 years. Table 1 provides the echogenic characteristics of the region of interest (ROI) identified by the radiologist that was utilized in the analysis. The table also identifies the carotid artery branch that was scanned where the plaque was subsequently excised using a carotid endarterectomy procedure. As listed in table 1, both symptomatic and asymptomatic patients were part of this study.

Patient scanning was performed as a standard clinical carotid examination, where the sonographer places the transducer on the skin surface at the location of carotid artery. The appropriate scan location was decided by the sonographer based on the surgical site for the patient, with only the ipsilateral side responsible for the symptom scanned. For the accumulated axial strain and lateral shift measurement, a VFX 13-5 linear array transducer was used. The center frequency of the transducer was set to the highest frequency possible with the transducer, i.e., 11.43 MHz. The lateral resolution was also set to the highest value, i.e. 508 A-lines for an image field width of 38 mm. The sampling rate for the RF signals was 40 MHz, and a single transmit focus was set at the depth of the plaque. Dynamic focusing was applied during echo reception. Only longitudinal scans obtained for the patient were post-processed.

The number of regions of interest selected in each patient depends on the presence of different plaque types identified based on their appearance in the B-mode images. In the

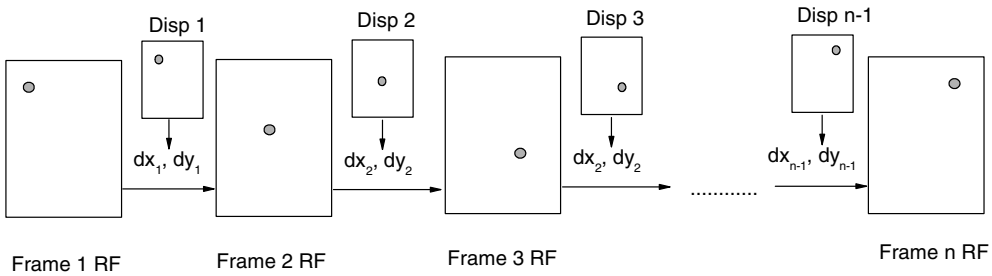

Figure 1. Illustration of the procedure using which the region of interest is tracked over all the frames within the cardiac cycle.

presence of different plaque types for the same patient, we label each region separately and include all regions in our analysis. On the other hand, if only a single type of plaque is visualized in the B-mode image of the patient, we choose the ROI corresponding to the region with the maximum stenosis. Although the same ROI could be present in several scans, we choose only one of the scans for analysis.

Parameter estimation

In vivo axial strain estimation. We have developed a 2D multi-level cross-correlation method for strain estimation for discontinuous tissue (Shi and Varghese 2007). Here, we utilize this technique to calculate the axial strain (strain estimated along the ultrasound propagation direction) distribution in plaques visualized within the carotid artery. The RF data file acquired contains frames over several cardiac cycles. Strain images are computed between consecutive frames using the 2D multilevel cross-correlation method. Since the frame rate is usually high (depends on system settings and is usually around 27 fps), displacement and strain estimates between two consecutive frames are quite small. However, the accumulated displacement and strain for an entire cardiac cycle can be quite large. The relative location of the plaque with respect to the vessel wall in the B-mode image may also move due to elevational and lateral motion of the plaque over the cardiac cycle. We therefore track the 2D displacement within ROIs selected within the plaque in both the axial and lateral directions (i.e. within the imaging plane). Since the ROI tracked may move both along the axial and lateral directions to different locations, we accumulate displacement values corresponding to each location to obtain the strain indices utilized for plaque characterization.

This procedure is illustrated in figure 1, where each large rectangle represents a RF data frame, with each of the smaller rectangles between the RF frames representing the calculated displacement map between the consecutive RF frames. The circle on the RF data frame represents the location of the ROI, with the corresponding circle on the displacement map denoting the calculated displacement value at the ROI position. Figure 1 exaggerates the displacement of the ROI to illustrate the concept. If the initial position of the first ROI is $P_1(x_1, y_1)$, and the calculated displacement at location P_1 between frames 1 and 2 for ROI_1 is $D_1(\text{d}x_1, \text{d}y_1)$, the new position of ROI is $P_2(x_1 + \text{d}x_1, y_1 + \text{d}y_1)$. After calculating the displacement between frames 2 and 3, the new displacement for this ROI is not at position P_1, instead, should be at P_2, we add the displacement vector $D_2(\text{d}x_2, \text{d}y_2)$ to obtain the new ROI location $P_3(x_1 + \text{d}x_1 + \text{d}x_2, y_1 + \text{d}y_1 + \text{d}y_2)$. Using this method, we can track the location of the ROI and thereby accumulate local displacements over frames within the cardiac cycle.

Estimation of a relative lateral shift between plaque and carotid artery wall. Some researchers have reported on the longitudinal movement and the resulting shear strain of the arterial wall over a cardiac cycle (Cinthio *et al* 2006, Haseyuki and Kanai 2007). In our study, we observe the presence of a relative lateral shift between arterial wall and plaque with the blood flow. Such long-term cyclic stretching and relaxation (fatigue) of the plaque may weaken the plaque–artery wall attachment and increase vulnerability to fracture. We hypothesize that the relative lateral motion between the plaque and the artery wall may be another important factor that would aid in the detection of plaque disruption or rupture. We therefore also estimate the relative lateral shift between plaque and carotid artery wall in the longitudinal scans obtained *in vivo* in the patients.

We utilized 2D cross-correlation analysis to track and calculate the relative lateral shift of the plaque during the cardiac cycle. We first manually select two ROIs, with one ROI within the plaque region and the second ROI on the artery wall in the B-mode image of the first frame in the sequence. Since we focus on the relative lateral shift, both ROIs have the same initial lateral position but different axial positions in the first B-mode image. We then utilize 2D cross-correlation to track the movement of each ROI through all frames in the sequence. Tracking was done to an accuracy of a single A-line in the lateral direction. The ROI size used in this analysis consisted of 64 points along the axial direction and 5 A-lines in the lateral direction (corresponding to a 1.2 mm $\times$ 0.4 mm ROI). The search range is usually 64 points in the axial direction (up or down) and 10 A-lines in the lateral direction (left or right).

To obtain sub-A-line accuracy in the lateral direction, we fit the 2D cross-correlation values around the maximum cross-correlation value to a 2D parabolic function $z = a + bx + cy + dx^2 + exy + fy^2$, where z is the cross-correlation coefficient, x and y denote the axial and lateral positions, respectively, and a to f represent the parameters of the fit. Using this fit of the cross-correlation function, we compute the position $(x_0 + \Delta x, y_0 + \Delta y)$ that corresponds to the maximum z value, theoretically the maximum cross-correlation value, to obtain the final relative lateral shift.

Results

Figure 2 presents (a) the B-mode image and (b) the axial strain image of a soft plaque embedded within the carotid artery wall for patient 9. Note that for the *in vivo* strain distribution depicted in figure 2(b) mid-gray depicts stiffer regions in the plaque and artery wall, while the brighter region depicts the location of the soft plaque within the carotid artery. The deformation and hence the axial strain within the soft plaque varies over the cardiac cycle (not shown) from dark to bright depending on the internal pressure induced due to blood flow over the cardiac cycle.

Figure 2(c) depicts the accumulated axial strain versus the frame number within the data loop over a ROI within the soft plaque region. The calculated ROI between frames i and $i + 1$ contains several strain pixels s and we obtain the mean strain $\bar{s}_i$ within the ROI. Since we acquire a series of RF data frames without gating, it is difficult to maintain the same starting location (for example, end diastole) for each data set precluding the use of a reference frame. In addition, since $\bar{s}_i$ is computed over consecutive frames in the data set, the accumulated mean strain of the ROI $\bar{S}_i = \sum_{j=1}^{i} \bar{s}_j$ is obtained, which may be either negative (compressive strains) or positive (strain during relaxation). We expect to see a periodic pattern of the accumulated strain $\bar{S}_i$ over the cardiac cycle, although the $\bar{S}_i$ value may be shifted depending on the location of the first frame within the cardiac cycle. The average value of accumulated strain over the entire acquired data set, which contains N frames, is calculated by $\tilde{S} = \frac{1}{N-1} \sum_{i=1}^{N-1} \bar{S}_i$.

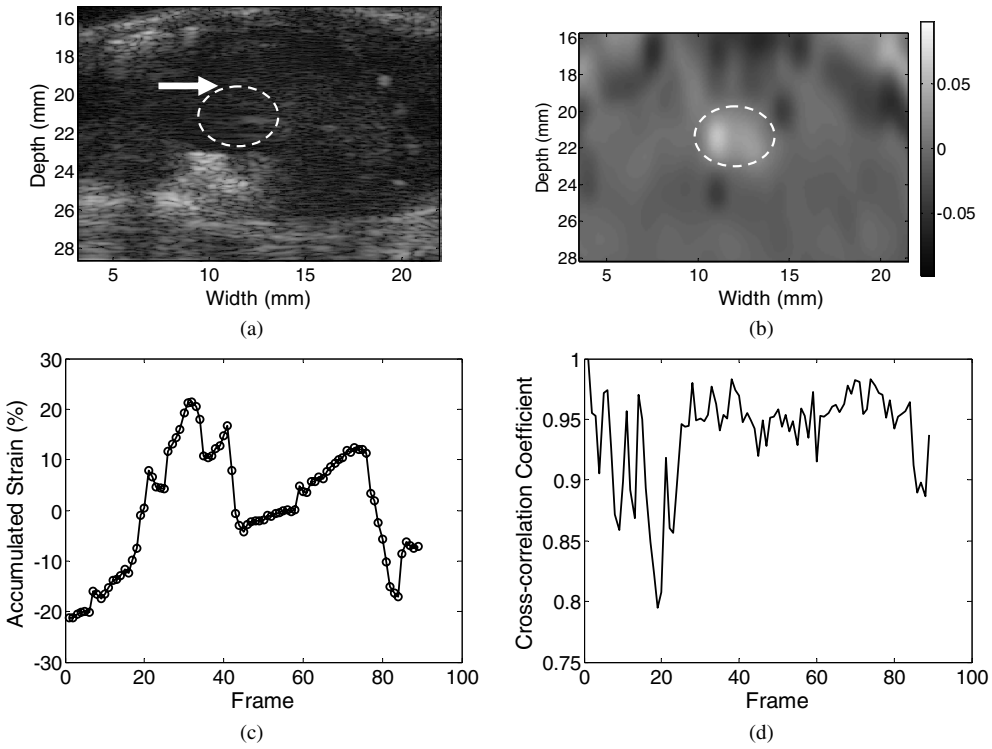

Figure 2. Region of the ultrasound B-mode image and accumulated axial strain for patient 9 with a soft plaque: (a) B-mode image of the soft plaque (the region marked by white arrow), (b) a typical axial strain image, (c) the accumulated axial strain versus frame number and (d) the cross-correlation coefficient versus frame number.

Figure 2(c) plots $\bar{S}_i - \tilde{S}$ versus frame number i ($i = 1, 2, \ldots, N-1$). The maximum accumulated strain is defined by the term $\max\{|\bar{S}_i - \tilde{S}|, i = 1, 2, \ldots, N-1\}$. The normalized correlation coefficient is included as a quantitative measure of the tracking success, where values above 0.9 indicate excellent tracking.

As shown in figure 2(c), the accumulated axial strain over consecutive frames is quite large, with the maximum accumulated strain around 20%. Meanwhile, observe that the frame strain could be as high as 6% as depicted in the colorbar of figure 2(b). Figure 2(d) presents the variation in the normalized cross-correlation coefficient over consecutive frames. During data acquisition for strain imaging, the frame rate was set to 27 fps. Therefore, in these plots, although the x-axes are labeled in units of frames, these units can be converted to time in 'seconds' by dividing by the frame rate.

In a similar manner, figure 3(a) presents the B-mode image of a heterogeneous region within a carotid plaque. Figure 3(b) depicts a typical axial strain image obtained using the 2D multi-level method. Figure 3(c) plots the accumulated axial strain versus the frame number. In this case, the maximum accumulated strain over consecutive frames is about 2%. Finally, the variation in the normalized cross-correlation coefficient of the ROI is shown in figure 3(d) over consecutive frames. Note that the bright region observed in figure 3(b) corresponds to a high-strain region within the heterogeneous plaque, which we hypothesize to be a soft plaque that undergoes relatively large deformations over the cardiac cycle. This bright region

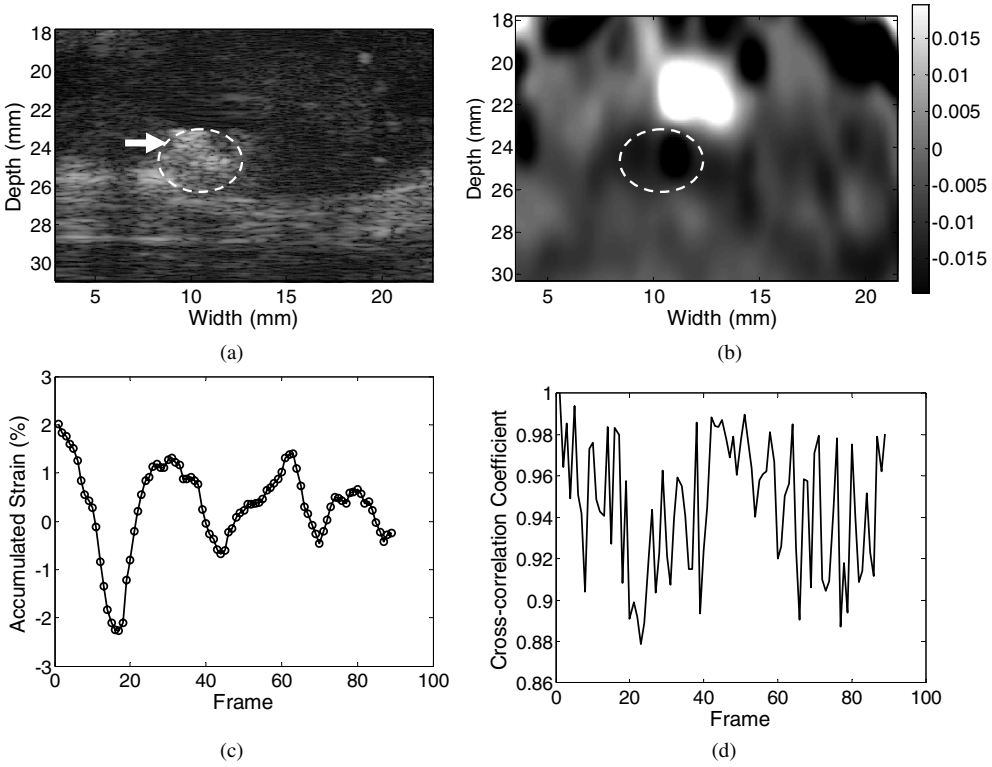

Figure 3. Region with a heterogeneous plaque on the ultrasound B-mode image and accumulated axial strain for the same patient: (a) B-mode image of heterogeneous plaque (the region marked by white arrow), (b) a typical axial strain image, (c) the accumulated axial strain versus frame number and (d) the cross-correlation coefficient versus frame number.

is the exact same ROI depicted in figure 2(b), the only difference being the scale utilized to emphasize the ROI with the stiffer plaque depicted in figure 3(b).

Finally, figure 4(a) presents a calcified region within *in vivo* carotid plaque, with a typical axial strain image shown in figure 4(b). However, for the calcified plaque, the strain image was calculated between frames 18 and 23 (5 frame difference), rather than consecutive frames. The reason for depicting the deformation over five frames is due to the fact that the frame strain between consecutive frames for this calcified plaque was too small to be easily tracked. Note that even after accumulation of deformation over five frames the strain value for the calcified region is only about 0.2%. Figure 4(c) plots the accumulated axial strain versus the frame number. We can clearly observe for the calcified region that the maximum accumulated axial strain is around 0.87%. Figure 4(d) presents the variation in the cross-correlation coefficient over consecutive frames.

Figures 5(a) and (b) present a histogram of the maximum accumulated axial strain for both calcified and soft plaques over all the patients in the study. Figure 5(a) clearly shows that the accumulated axial strain values are mostly small for calcified plaques. On the other hand, figure 5(b) shows that the accumulated axial strains span from small values to large values, i.e. about 20% for softer plaques.

In some of our *in vivo* results for the estimation of the relative lateral shift, we found that the relative shift is a combination of a cyclic waveform and a general trend. The cyclic

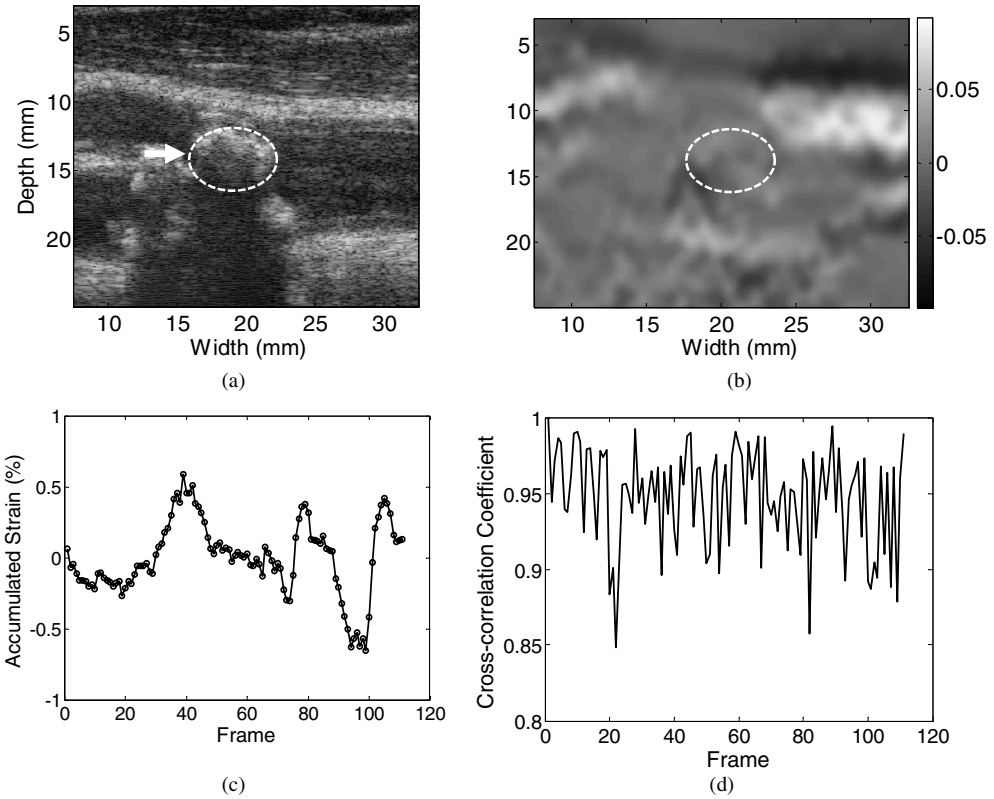

Figure 4. Ultrasound B-mode image and accumulated axial strain for patient 3 with a calcified plaque: (a) B-mode image of the calcified plaque (the region marked by white dashed circle), (b) a typical strain image, (c) the accumulated axial strain versus number of frames and (d) the cross-correlation coefficient versus number of frames.

waveform is due to the variations with the cardiac cycle, while the general trend could be due to several factors. When the transducer is placed on the patient's neck, small shifts in the position of the transducer can arise from the sliding of the transducer on the skin surface, due to (i) the ultrasound gel used for coupling makes the transducer and skin interaction to be slippery and (ii) for carotid examinations the sonographers hold the transducer with minimal force on the skin surface over the entire data acquisition (several seconds), which could introduce some motion between the transducer and skin surface. Besides possible sliding of the transducer, it is also possible that patient's motion would exist although we request that the patients hold their breath and not move during the data acquisition. However, these shifts are relatively small ($\sim$1 mm over entire data acquisition). Although the plaque and artery wall would move in synchrony under these conditions, the imaged plane and hence tracked regions may shift as a result.

In these cases, assuming a linear trend we use a straight line to fit and remove the general trend from the signal. An example is shown in figure 6, depicting the relative lateral motion of a calcified plaque in patient 2. Note the presence of the linear trend added to the cyclic waveform. After removing this linear trend, figure 6(b) depicts only the cyclic waveform, over which we estimate the relative lateral shift for the calcified plaque. This shift is 0.71 mm from the peak to the valley over one cardiac cycle for this patient.

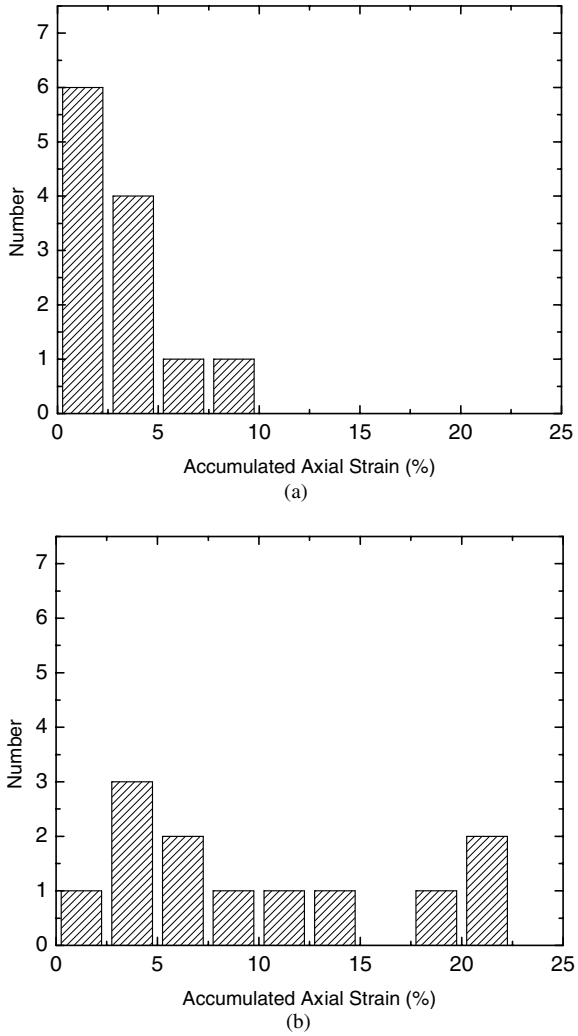

Figure 5. Histogram of the accumulated axial strain of (a) calcified plaques and (b) soft plaques.

From figure 7(a), we observe that most of the plaques identified as calcified by the radiologist demonstrate only small amounts of relative lateral shifts with respect to the artery wall, with none of them indicating a larger than 1 mm relative shift. On the other hand, the histograms shown in figure 7(b) indicate that softer plaques undergo increased lateral motion or displacement with blood flow during the cardiac cycle. For softer plaques the relative lateral shifts can vary in a larger range, from relatively small lateral shifts to lateral shifts of up to 2–3 mm.

Finally, figure 8 presents a plot of the maximum relative lateral shift versus the maximum accumulated axial strain for all the plaque ROIs identified by the radiologist for all patients. Observe from the figure that calcified plaques in general present with smaller values of both the maximum relative lateral shift and maximum accumulated axial strains, while softer plaques exhibit a wider range in the values of the two strain indices discussed in this paper.

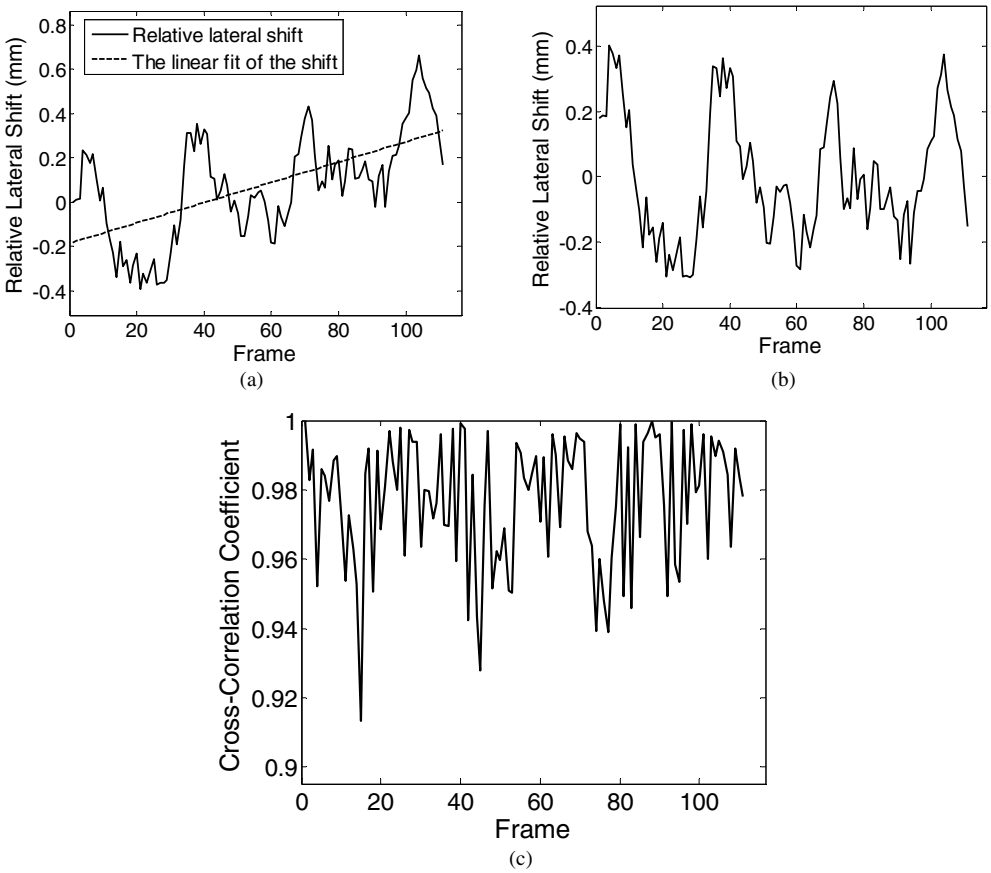

Figure 6. (a) Relative lateral shift between plaque and artery wall and the linear fit of this shift to detrend the data; (b) the relative lateral shift between plaque and artery wall with general linear trend removed; (c) the 2D cross-correlation coefficient for the ROI.

Receiver operating characteristics

Receiver operating characteristic (ROC) analysis is used in this study to evaluate the sensitivity and specificity of the two strain indices. For the ROC analysis, a reference metric for the plaque differentiation is necessary. Although histological results corresponding to the scanned segment would best serve as the reference metric, this is difficult in practical situations, since the plaque structure is usually damaged during surgical endarterectomy procedure. On the other hand, many researchers have demonstrated that ultrasound B-mode characterization of plaque may provide valuable information to assess the atherosclerotic lesion (Meairs and Hennerici 1999, Sabetai *et al* 2000, Gronholdt *et al* 2001, AbuRahma *et al* 2002, Kern *et al* 2004). Differentiation between homogeneous calcified plaques from other homogeneous plaque types is easily addressed with B-mode images (Gronholdt *et al* 1998). Echolucent or hypoechoic plaques (plaque identified as non-calcified in our analysis) that causes a 50% or greater stenosis were also associated with an increased incidence of stroke and thereby candidates for carotid endarterectomy procedures (Gronholdt *et al* 1998). In addition, hypoechoic plaques were more likely to be symptomatic than hyperechoic

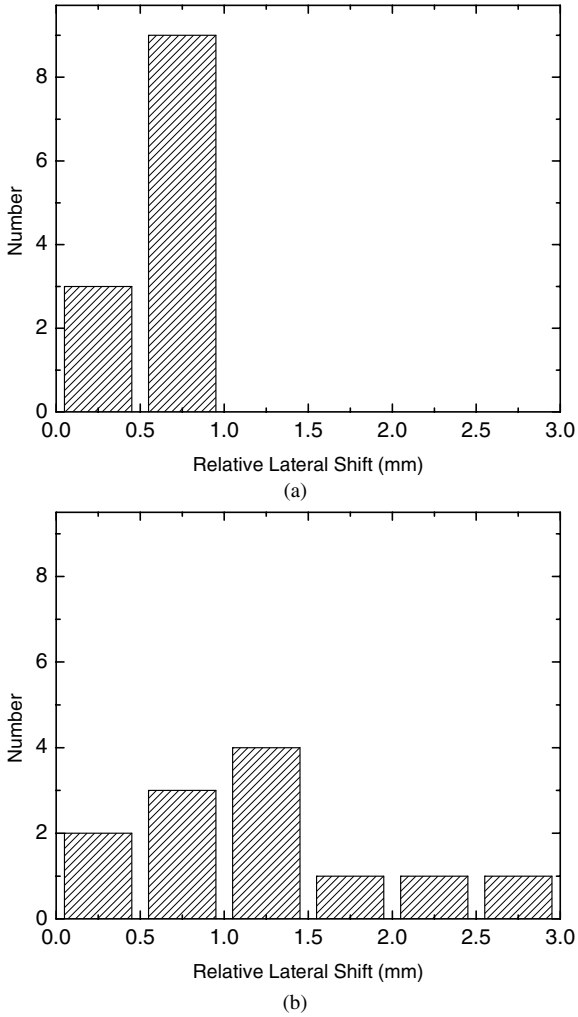

Figure 7. Histograms for the relative lateral shifts between plaque and artery wall ROIs, respectively: (a) calcified plaque and (b) soft plaque.

ones (Sabetai *et al* 2000). Another important conclusion was that heterogeneous plaques were more strongly associated with symptoms than homogeneous plaques for all stenoses grades (AbuRahma *et al* 2002). We therefore utilize the radiologist identification of soft or calcified regions on the B-mode image, which is the current standard of care as the reference metric.

In this ROC analysis, we arbitrarily choose calcified plaque as the 'True' category. For each ROI, we label the calculated maximum accumulated axial strain as S, so for N ROIs, we have a collection of maximum accumulated axial strain values $\{S_i, i = 1, 2, \ldots, N\}$. Now if we move the maximum accumulated axial strain parameter S' from $\min\{S_i, i = 1, 2, \ldots, N\}$ to $\max\{S_i, i = 1, 2, \ldots, N\}$, for each S', we compare it with the S value. If $S > S'$, we make the decision that the sample is calcified (i.e., positive). The true positive fraction (TPF) represents the ratio of sample number in the True category that also tested as positive versus

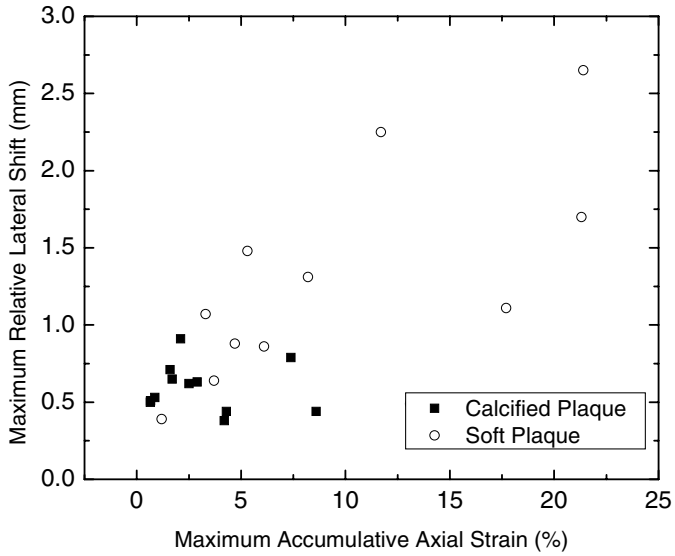

Figure 8. Plot of the maximum relative lateral shift versus the maximum accumulated axial strain for both calcified plaque and soft plaque.

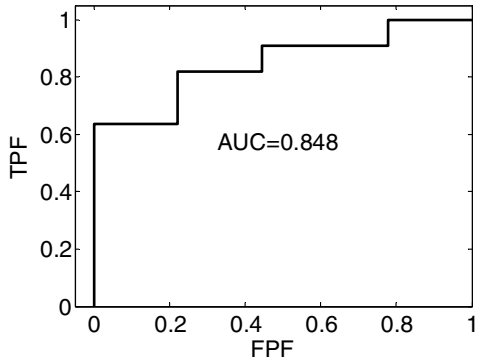

Figure 9. ROC curve for the maximum accumulated axial strain estimated from the *in vivo* plaque data.

the total number in the True category. Similarly, the false positive fraction (FPF) represents the ratio of the sample number in False category that tested as positive versus the total number in the False category; obviously, TPF and FPF are functions of the moving threshold value S'.

The ROC curve for the maximum accumulated axial strain parameter is plotted in figure 9. The area under the curve (AUC) for the maximum accumulated axial strain parameter obtained was 0.848. Therefore, the maximum accumulated axial strain appears to be a fair parameter to differentiate between non-calcified and calcified plaque. In a similar manner, figure 10 plots the ROC curve for the maximum relative lateral shift. The AUC value equals 0.869, which indicates that the maximum relative lateral shift value is also a fair criterion to differentiate between non-calcified and calcified plaque.

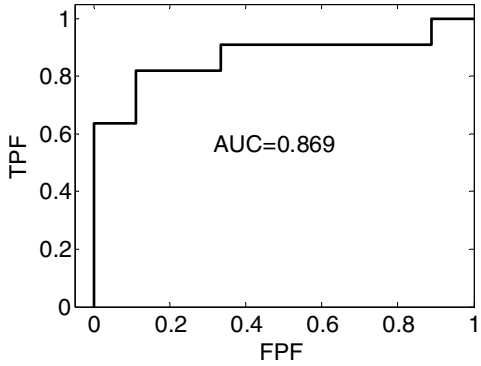

Figure 10. ROC curve of the maximum relative lateral shift parameter estimated from the *in vivo* plaque data.

Discussion

In this paper, we evaluate two strain indices, namely, the accumulated axial strain and the maximum relative lateral shifts for *in vivo* carotid atherosclerotic artery plaque characterization. *In vivo* characterization of the carotid plaque is difficult since the carotid artery and plaque are embedded within several tissue layers: between the ultrasound transducer and carotid plaque that include skin, fat, muscle tissue, artery wall and blood. Ultrasound beam refraction and reflection are factors that complicate power spectral analysis and speckle tracking of plaque tissue. In addition, patient motion and respiratory artifacts introduce errors into the axial strain and lateral relative shifts estimated.

Results in the literature for *in vivo* carotid strain imaging have reported on the utilization of different strain components to characterize plaque tissue based on their stiffness characteristics. Strain imaging along both the cross-sectional and longitudinal directions have been reported in the carotid artery (Ribbers *et al* 2007). However, cross-sectional imaging is more challenging since the radial and circumferential strains are not well aligned with the ultrasound beam for all regions. On the other hand, for longitudinal scans the radial strain and the ultrasound beam are either aligned or at a specific angle, which makes the observed strain component to be easily interpreted for the given geometries and boundary conditions (Ribbers *et al* 2007). Other investigators have reported on the estimation of quantitative parameters, such as Young's modulus, by solving the inverse problem using estimated strains and modeling of the carotid artery (Schmitt *et al* 2007). Strain imaging within the carotid artery is affected by hemodynamic parameters that vary significantly in the presence of stenosis and have to be accurately modeled if the modulus is desired.

In addition, axial strain images of the plaque and the carotid artery vary over the entire cardiac cycle, and variations over the entire cardiac cycle have to be evaluated. Axial strain distributions obtained from consecutive frames referred to as frame strains (plotted in figures 2–4(b)) may provide only a snapshot of the strain distribution. In this paper, we evaluate and report on the variation of two strain indices, namely, the maximum accumulated axial strain and the maximum relative lateral shift over small ROI placed in the plaque over the entire cardiac cycle.

For *in vivo* axial strain estimation, we observe several cases where non-calcified hypoechoic plaques exhibit more than 20% accumulated strain over a cardiac cycle. This

suggests these plaques are easily deformed by the pulsation of blood and flow during the cardiac cycle. On the other hand, calcified plaques exhibit only moderate amounts of accumulated axial strain (∼5%) during blood flow pulsations. Therefore, the accumulated axial strain parameter can by itself provide useful information regarding the elastic properties of plaque.

Due to a relatively low pitch of the transducer elements in the lateral direction compared to the axial sampling rate, the accumulated lateral strain includes additional noise artifacts. We therefore estimate the relative lateral shift or displacement between the plaque and artery wall to characterize calcified and soft plaques. Soft plaques demonstrate significantly larger relative lateral shift values than calcified plaques in the small number of patients studied. This result suggests that softer plaques are more easily stretched or compressed and also move laterally in the carotid artery during the cardiac cycle. In contrast, calcified plaques usually stay in their location and do not stretch to the degree that soft plaques do. Quantitatively, the relative lateral shift between soft plaques and the artery wall were as high as 2–3 mm, while the lateral shifts of calcified plaques were usually under 1 mm.

Observe, from figure 7, that some of the calcified and non-calcified hypoechoic plaques show a few cases with relative lateral shifts around 0.75 mm. These results indicate that additional parameters may be required to clearly differentiate between plaque types. On the other hand, these results could also point to cases where the deformation of the plaque over the cardiac cycle may not be large enough to induce plaque rupture. Clearly, the sensitivity and specificity of these deformation parameters or strain indices have to be evaluated over a large study along with pathological confirmation of the plaque type.

Conclusion

In conclusion, preliminary *in vivo* based strain indices, namely, the maximum accumulated axial strain and the maximum relative lateral shift results provide promising differentiation between non-calcified and calcified plaques. Since softer plaques are more likely to be unstable or vulnerable plaques when compared to calcified plaques, these strain indices have the potential to be utilized as a screening tool for the detection of vulnerable plaque.

Acknowledgments

We are grateful to Professors James A Zagzebski and Timothy Hall for insightful conversations regarding acoustic scattering physics and modeling of soft tissues. The authors would also like to thank Ms Pam Winne, for the co-ordination and scheduling of the patients for this study. This work is supported in part by start-up funds from the University of Wisconsin-Madison Medical School and Graduate School and NIH grant R21 EB003853. Mr McCormick is supported by Grant Numbers T90DK070079 and R90DK071515 from the National Institute of Diabetes and Digestive and Kidney Diseases.

References

AbuRahma A F, Wulu J T Jr and Crotty B 2002 Carotid plaque ultrasonic heterogeneity and severity of stenosis *Stroke* **33** 1772–5

Baldewsing R A, Schaar J A, Mastik F, Oomens C W and van der Steen A F 2005 Assessment of vulnerable plaque composition by matching the deformation of a parametric plaque model to measured plaque deformation *IEEE Trans. Med. Imaging* **24** 514–28

Bertrand M, Meunier M, Doucet M and Ferland G 1989 Ultrasonic biomechanical strain gauge based on speckle tracking *IEEE Ultrasonics Symp.* pp 859–64

Bridal S L, Fornes P, Bruneval P and Berger G 1997 Correlation of ultrasonic attenuation (30 to 50 MHz) and constituents of atherosclerotic plaque *Ultrasound Med. Biol.* **23** 691–703

Cespedes E I 1993 Elastography: imaging of biological tissue elasticity *PhD Dissertation* University of Houston, Texas

Chen E J, Jenkins W K and O'Brien W D Jr 1995 Performance of ultrasonic speckle tracking in various tissues *J. Acoust. Soc. Am.* **98** 1273–8

Cinthio M, Ahlgren A R, Bergkvist J, Jansson T, Persson H W and Lindstrom K 2006 Longitudinal movements and resulting shear strain of the arterial wall *Am. J. Physiol. Heart Circ. Physiol.* **291** H394–402

de Korte C L and van der Steen A F 2002 Intravascular ultrasound elastography: an overview *Ultrasonics* **40** 859–65

de Korte C L, van der Steen A F, Cepedes E I, Pasterkamp G, Carlier S G, Mastik F, Schoneveld A H, Serruys P W and Bom N 2000 Characterization of plaque components and vulnerability with intravascular ultrasound elastography *Phys. Med. Biol.* **45** 1465–75

Doyley M M, Bamber J C, Fuechsel F and Bush N L 2001 A freehand elastographic imaging approach for clinical breast imaging: system development and performance evaluation *Ultrasound Med. Biol.* **27** 1347–57

Droste D W, Decker W, Siemens H J, Kaps M and Schulte-Altedorneburg G 1996 Variability in occurrence of embolic signals in long term transcranial Doppler recordings *Neurol. Res.* **18** 25–30

Emelianov S Y, Chen X, O'Donnell M, Knipp B, Myers D, Wakefield T W and Rubin J M 2002 Triplex ultrasound: elasticity imaging to age deep venous thrombosis *Ultrasound Med. Biol.* **28** 757–67

Fuster V, Stein B, Ambrose J A, Badimon L, Badimon J J and Chesebro J H 1990 Atherosclerotic plaque rupture and thrombosis: evolving concepts *Circulation* **82** II47–59

Gao L, Parker K J, Lerner R M and Levinson S F 1996 Imaging of the elastic properties of tissue—a review *Ultrasound Med. Biol.* **22** 959–77

Garra B S, Cespedes E I, Ophir J, Spratt S R, Zuurbier R A, Magnant C M and Pennanen M F 1997 Elastography of breast lesions: initial clinical results *Radiology* **202** 79–86

Golemati S, Sassano A, Lever M J, Bharath A A, Dhanjil S and Nicolaides A N 2003 Carotid artery wall motion estimated from B-mode ultrasound using region tracking and block matching *Ultrasound Med. Biol.* **29** 387–99

Gronholdt M L 1999 Ultrasound and lipoproteins as predictors of lipid-rich, rupture-prone plaques in the carotid artery *Arterioscler. Thromb. Vasc. Biol.* **19** 2–13

Gronholdt M L, Nordestgaard B G, Schroeder T V, Vorstrup S and Sillesen H 2001 Ultrasonic echolucent carotid plaques predict future strokes *Circulation* **104** 68–73

Gronholdt M L, Nordestgaard B G, Wiebe B M, Wilhjelm J E and Sillesen H 1998 Echo-lucency of computerized ultrasound images of carotid atherosclerotic plaques are associated with increased levels of triglyceride-rich lipoproteins as well as increased plaque lipid content *Circulation* **97** 34–40

Haseyuki H and Kanai H 2007 Strain imaging of arterial wall with translational motion compensation and error correction *IEEE Ultrasonics Symp.* pp 860–3

Insana M F, Cook L T, Bilgen M, Chaturvedi P and Zhu Y 2000 Maximum-likelihood approach to strain imaging using ultrasound *J. Acoust. Soc. Am.* **107** 1421–34

Kallel F and Bertrand M 1996 Tissue elasticity reconstruction using linear perturbation method *IEEE Trans. Med. Imaging* **15** 299–313

Kern R, Szabo K, Hennerici M and Meairs S 2004 Characterization of carotid artery plaques using real-time compound B-mode ultrasound *Stroke* **35** 870–5

Konofagou E and Ophir J 1998 A new elastographic method for estimation and imaging of lateral displacements, lateral strains, corrected axial strains and Poisson's ratios in tissues *Ultrasound Med. Biol.* **24** 1183–99

Krouskop T A, Dougherty D R and Vinson F S 1987 A pulsed Doppler ultrasonic system for making noninvasive measurements of the mechanical properties of soft tissue *J. Rehabil. Res. Dev.* **24** 1–8

Leung K Y E, Baldewsing R A, Mastik F, Schaar J A, Gisolf A and van der Steen A F W 2006 Motion compensation for intravascular ultrasound palpography *IEEE Trans. Ultrason. Ferroelectr. Freq. Control* **53** 1269–80

Maurice R L, Fromageau J, Brusseau E, Finet G, Rioufol G and Cloutier G 2007 On the potential of the Lagrangian estimator for endovascular ultrasound elastography: *in vivo* human coronary artery study *Ultrasound Med. Biol.* **33** 1199–205

Maurice R L, Ohayon J, Fretigny Y, Bertrand M, Soulez G and Cloutier G 2004 Noninvasive vascular elastography: theoretical framework *IEEE Trans. Med. Imaging* **23** 164–80

Maurice R L, Soulez G, Giroux M F and Cloutier G 2008 Noninvasive vascular elastography for carotid artery characterization on subjects without previous history of atherosclerosis *Med. Phys.* **35** 3436–43

Meairs S and Hennerici M 1999 Four-dimensional ultrasonographic characterization of plaque surface motion in patients with symptomatic and asymptomatic carotid artery stenosis *Stroke* **30** 1807–13

Nair A, Kuban B D, Tuzcu E M, Schoenhagen P, Nissen S E and Vince D G 2002 Coronary plaque classification with intravascular ultrasound radiofrequency data analysis *Circulation* **106** 2200–6

Nightingale K, Scott Soo M, Nightingale R and Trahey G 2002 Acoustic radiation force impulse imaging: *in vivo* demonstration of clinical feasibility *Ultrasound Med. Biol.* **28** 227–35

Noritomi T, Sigel B, Swami V, Justin J, Gahtan V, Chen X, Feleppa E J, Roberts A B and Shirouzu K 1997 Carotid plaque typing by multiple-parameter ultrasonic tissue characterization *Ultrasound Med. Biol.* **23** 643–50

O'Donnell M, Skovoroda A R and Shapo B M 1991 Measurement of arterial wall motion using Fourier based speckle tracking algorithms *Proc IEEE Ultrasonics Symp.* pp 1101–4

O'Donnell M, Skovoroda A R, Shapo B M and Emelianov S Y 1994 Internal displacement and strain imaging using ultrasonic speckle tracking *IEEE Trans. Ultrason. Ferroelectr. Freq. Control* **41** 314–25

Ophir J, Cespedes I, Ponnekanti H, Yazdi Y and Li X 1991 Elastography: a quantitative method for imaging the elasticity of biological tissues *Ultrason. Imaging* **13** 111–34

Ophir J, Garra B, Kallel F, Konofagou E, Krouskop T, Righetti R and Varghese T 2000 Elastographic imaging *Ultrasound Med. Biol.* **26** (Suppl.) S23–9

Parker K J, Gao L, Lerner R M and Levinson S F 1996 Techniques for elastic imaging: a review *IEEE Eng. Med. Biol. Mag.* **15** 52–9

Parker K J, Huang S R, Musulin R A and Lerner R M 1990 Tissue response to mechanical vibrations for 'sonoelasticity imaging' *Ultrasound Med. Biol.* **16** 241–6

Ribbers H, Lopata R G, Holewijn S, Pasterkamp G, Blankensteijn J D and de Korte C L 2007 Noninvasive two-dimensional strain imaging of arteries: validation in phantoms and preliminary experience in carotid arteries *in vivo Ultrasound Med. Biol.* **33** 530–40

Richardson P D 2002 Biomechanics of plaque rupture: progress, problems, and new frontiers *Ann. Biomed. Eng.* **30** 524–36

Richardson P D, Davies M J and Born G V 1989 Influence of plaque configuration and stress distribution on fissuring of coronary atherosclerotic plaques *Lancet* **2** 941–4

Rubin J M, Xie H, Kim K, Weitzel W F, Emelianov S Y, Aglyamov S R, Wakefield T W, Urquhart A G and O'Donnell M 2006 Sonographic elasticity imaging of acute and chronic deep venous thrombosis in humans *J. Ultrasound Med.* **25** 1179–86

Sabetai M M, Tegos T J, Nicolaides A N, El-Atrozy T S, Dhanjil S, Griffin M, Belcaro G and Geroulakos G 2000 Hemispheric symptoms and carotid plaque echomorphology *J. Vasc. Surg.* **31** 39–49

Schmitt C, Soulez G, Maurice R L, Giroux M F and Cloutier G 2007 Noninvasive vascular elastography: toward a complementary characterization tool of atherosclerosis in carotid arteries *Ultrasound Med. Biol.* **33** 1841–58

Shi H 2007 Atherosclerotic carotid plaque characterization using ultrasound and elastography *PhD Dissertation* University of Wisconsin-Madison, Madison

Shi H, Chen Q and Varghese T 2005 A general solution for catheter position effects for strain estimation in intravascular elastography *Ultrasound Med. Biol.* **31** 1509–26

Shi H, Mitchell C C, Salamat M S, Kliewer M A, Dempsey R J, Klug M, Leist C and Varghese T 2006 Elastographic characterization of atherosclerotic carotid plaque *in vivo Proc. 51st Annual Convention (American Institute of Ultrasound in Medicine, Washington DC, District of Columbia)*

Shi H and Varghese T 2007 Two-dimensional multi-level strain estimation for discontinuous tissue *Phys. Med. Biol.* **52** 389–401

Shi H, Varghese T, Dempsey R J, Salamat M S and Zagzebski J A 2008 Relationship between ultrasonic attenuation, size and axial strain parameters for *ex vivo* atherosclerotic carotid plaque *Ultrasound Med. Biol.* **34** 1666–77

Siebler M, Sitzer M, Rose G and Steinmetz H 1996 Microembolism in carotid artery disease *Echocardiography* **13** 529–36

Sumi C, Suzuki A and Nakayama K 1995 Estimation of shear modulus distribution in soft tissue from strain distribution *IEEE. Trans. Biomed. Eng.* **42** 193–202

Talhami H E, Wilson L S and Neale M L 1994 Spectral tissue strain: a new technique for imaging tissue strain using intravascular ultrasound *Ultrasound Med. Biol.* **20** 759–72

van der Steen A F, de Korte C L and Cespedes E I 1998 Intravascular ultrasound elastography *Ultraschall. Med.* **19** 196–201

Varghese T, Ophir J, Konofagou E, Kallel F and Righetti R 2001 Tradeoffs in elastographic imaging *Ultrason. Imaging* **23** 216–48

Walker W F, Fernandez F J and Negron L A 2000 A method of imaging viscoelastic parameters with acoustic radiation force *Phys. Med. Biol.* **45** 1437–47

Waters K R, Bridal S L, Cohen-Bacrie C, Levrier C, Fornes P and Laugier P 2003 Parametric analysis of carotid plaque using a clinical ultrasound imaging system *Ultrasound Med. Biol.* **29** 1521–30

Weitzel W F, Kim K, Rubin J M, Xie H and O'Donnell M 2005 Renal advances in ultrasound elasticity imaging: measuring the compliance of arteries and kidneys in end-stage renal disease *Blood Purif.* **23** 10–7

Wilson L S, Neale M L, Talhami H E and Appleberg M 1994 Preliminary results from attenuation-slope mapping of plaque using intravascular ultrasound *Ultrasound Med. Biol.* **20** 529–42

Wilson L S and Robinson D E 1982 Ultrasonic measurement of small displacements and deformations of tissue *Ultrason. Imaging* **4** 71–82

Yamakoshi Y, Sato J and Sato T 1990 Ultrasonic Imaging of internal vibration of soft tissue under forced vibration *IEEE Trans. Ultrason. Ferroelectr. Freq. Control* **37** 45–53

Zhu Y and Hall T J 2002 A modified block matching method for real-time freehand strain imaging *Ultrason. Imaging* **24** 161–76